Interpretation of the band-structure results for elastic and acoustic waves by analogy with the LCAO approach

M. Kafesaki and E. N. Economou
Research Center of Crete, Foundation for Research and Technology-Hellas, P.O. Box 1527, 71110 Heraklio, Crete, Greece and Department of Physics, University of Crete, Crete, Greece
(Received 9 March 1995; revised manuscript received 26 July 1995)

The band-structure results for elastic and acoustic waves propagating in a composite (consisting of periodically placed spheres in a host material) are analyzed by employing the frequency dependence of the scattering cross section from a single sphere. Two limiting modes of propagation can be visualized. According to the first the wave propagates mainly through the host material; according to the second the wave hops coherently from a sphere to its neighbors using the resonances in the single-sphere scattering cross section. This second mode is the analog of the linear combination of atomic orbitals in electronic propagation, with the atomic orbitals replaced by the resonances.

I. INTRODUCTION

There has been growing interest in recent years in the propagation of classical waves[1,2] (CW) such as electromagnetic[3–14] (EM) , acoustic[15,16] (AC, in fluids) and elastic[15–20] (EL, in solids) in composite materials either periodic or random. The interest in CW in periodic materials, is mainly connected to the question of the existence or not of spectral gaps (stop bands). This same question applied to the electron waves, constitutes the heart of solid-state physics and has been studied extensively over the last 65 years.

However, CW propagation in composites, where each component allows free propagation, presents novel aspects not encountered in electron waves: (i) The classical wave equation, $\nabla^2\phi+[\omega^2/c^2(\mathbf{r})]\phi=0$, is equivalent with Shrödinger's equation, $\nabla^2\phi+2[E-V(\mathbf{r})]\phi=0$, if and only if, the corresponding electronic energy E is higher than the maximum value of the potential $V(\mathbf{r})$. In that energy region localization of the electrons (for random systems) or spectral gaps (for periodic systems) do not appear easily, although systematic examination of the problem has not been done (at least for the random case). (ii) The vector character of EM and EL waves plays an important and novel role in connection with the question of spectral gaps. (iii) The spatial variation of the mass density entering the equations for AC and EL waves, modifies the wave equation in a nontrivial way introducing the possibility of novel behavior such as the exclusion of the wave from one of the two components of the binary by allowing the density ratio to be much larger or much smaller than unity (while the velocity ratio remains fixed). The interest in spectral gaps for CW stems from the possibility of tailoring the EM, AC, and EL spectrum and thus possibly repeating with photons or even phonons some of the wonderful things that have been done with electrons in semiconductors.

CW also possess many advantages over electron waves for the study of their propagation in random media and especially for checking experimentally the disorder-induced transition from propagating to localized eigenstates. Such a transition, although very important for the transport properties of many materials, cannot be studied experimentally in an unambiguous way for electron waves because of the difficulty of fixing the electronic energy and because of the interactions among electrons and phonons. In contrast, for CW, the frequency can be chosen accurately and easily and the complications due to interactions are absent (at least for weak fields). However, one has to overcome the difficulty of constructing composites sustaining localized CW.

The solution of this last problem was greatly facilitated by the suggestion by John and Rangarajan[1] and by Economou and Zdetsis[2] that the existence of a band of localized eigenstates in a random system is directly related to the existence of spectral gaps in a periodic system, since both are due to destructive interference of multiple scattered waves. Indeed, by gradually disordering a periodic system possessing gaps, we create tails of localized eigenstates within the gap. This was the main reason for the initial revival of interest in CW propagating within periodic media.

Scalar waves were the first to be studied.[3,21] It was found[1,2,21,22] that the main parameters determining the appearance or not of band gaps and of bands of localized eigenstates were the *volume fraction* of one of the components of the binary composite structure and the *ratio of velocities* of propagation in each component of the system. Indeed, the velocity of propagation ratio between the two components of the composite medium must exceed a certain threshold value and the volume fraction of the low velocity component must be in a certain range which depends on the topology and the geometry of the composite structure for gaps to appear.

Other factors such as the topology (whether the low velocity component consists of isolated inclusions — cermet topology — or forms a continuous network-network topology), the lattice structure, and other geometrical characteristics were found to play a role too.

Led by the experiment of Yablonovitch and Gmitter,[5] attention was directed to the possible existence of gaps in the propagation of EM waves in periodic composite structures (where one of the components may be just air). Although the conditions for gaps in the EM case were more severe than those in the scalar case, structures were found computationally[6–8] and constructed experimentally (see, e.g.,

the article by Yablonovitch in Ref. 11), exhibiting gaps up to the 10^{12} Hz range.[23] The coupling between the two components of the EM wave, through a term involving $\nabla \cdot \mathbf{E}$, seems[20] to be responsible for some notable differences from the scalar case such as the preference for the network topology.

Acoustic (ACW) and elastic waves (ELW) attracted attention in connection with the gap or localization possibility[15,16] not only because of their many applications but for their rich physics as well. The latter stems from the enormous variety of easily constructed structures, the appearance of a term proportional to $\nabla\rho\nabla \cdot \mathbf{u}$ (where $\mathbf{u}$ is the acoustic field displacement and ρ is the mass density) and the full vector character of the elastic case with various velocity ratio between the longitudinal and the transverse components. The wealth of computational[15,16,18–20] and experimental[24,25,17] data which have been accumulated regarding the midgap frequency, the size of the gap and its dependence on the various parameters need further physical interpretations.

For all types of CW it has been found that:

(i) The material corresponding to low propagation velocity embedded in a high propagation velocity matrix is a more efficient scatterer than the inverse arrangement, *everything else being the same*. This is not surprising since low propagation velocity corresponds to negative potential in the electronic case. It is well known (in the electronic case) that a negative scattering potential may exhibit strong peaks (resonances) in the scattering cross section.

(ii) The higher the velocity ratio between the two components of the composite, the more favorable the condition for gaps (although saturation appears for very high values of this ratio).

(iii) The volume fraction occupied by the low velocity component must be in a certain range for gaps to exist. For AC and EL waves, in three-dimensional structures, this range is usually around the 10 – 20% mark (although higher values have been observed[17]), while for EM higher values up to 50% have been found. The higher the ratio $\omega_g a/c$, the higher the favorable volume fraction tends to be (ω_g is the midgap frequency, a is the sphere radius, and c is the wave velocity).

(iv) AC and EL waves seem to prefer in most cases the cermet topology, while the network topology gives better results for EM waves.

(v) For AC and EL waves, besides the velocity contrast, the density contrast is very important. However, for AC waves low-density scatterers (i.e., low-density inclusions in a high-density matrix) favor gaps, while for EL waves high-density inclusions in a low-density matrix is the preferable setup.

(vi) For EL waves the ratio of longitudinal to transverse velocities (c_l/c_s) in each component is another parameter; usually the smaller this ratio the better for gap creation, although the dependence on this parameter in some cases appears more complicated and less clear.

Considerable success in understanding the above results for simple scalar classical waves (corresponding to ACW and constant density) was achieved by considering a plane wave scattered by a single inclusion and by connecting the strong resonances in this scattering cross section with the appearance of gaps. In this way the position as well as the size of the gap can be estimated[2,26] by the position and the magnitude of the first few strong resonances which occur when half the wavelength within the inclusion medium is comparable to an integer times its linear size. By considering also the condition for Bragg interference of these strongly scattered waves, one obtains a rough estimate of the optimum volume fraction. Similar analysis was used to interpret the appearance and the size of the gaps for EM wave propagation,[26] although the connection is more complicated probably because of the vector character of the EM waves.

In the present paper we attempt the same approach of connecting the multiple-scattering-induced gaps with strong resonances in the single-scattering cross section for AC and EL waves. For this purpose we calculate the scattering cross section for a plane ACW and ELW scattered by a single-spherical inclusion. We compare the features of this cross section with previous band-structure results[18–20] in periodic composites, checking thus the connection between the two and possibly interpreting the existing results, especially the puzzling observation of the mass density contrast in fluids and in solids.

II. MODEL AND METHODS OF CALCULATION

As was mentioned above, the main part of the present work is the calculation of the scattering cross sections by a single-spherical inclusion and their possible connection with spectral gaps in periodic composites.

This calculation was done by Yiang and Truell.[27–29] Also Gaunaurd and co-workers[30,31] (see also Ref. 32) have worked extensively on the scattering from a single-spherical inclusion.

Here, we calculate this cross section following mainly Straton's[33] notation and formulas. We apply these formulas, among other systems, to a combination of matrix scatterer for which band-structure results in composites are available.[15,16,18–20,34] In Appendix B we write explicitly the rather complicated formulas for the cross section for completeness (and because of a few misprints in the existing literature regarding these formulas).

We shall present the analytical results for the case where the two materials (matrix-inclusion) are solids. Liquids, in computational work, can be treated as solids with shear wave velocity almost equal to zero.

We consider two types of incident wave propagating in the $\hat{\mathbf{z}}$ direction and incident on the surface of the sphere. (a) a longitudinal plane wave (L scattering), (b) a shear (transverse) plane wave polarized in the $\hat{\mathbf{x}}$ direction (S scattering).

For the calculation of the scattering cross section which is defined as the scattered energy flux to the incident energy flux per unit area, the knowledge of the scattered wave and the wave inside the sphere is necessary. The above waves result from partial solutions of the elastic wave equation with application of proper boundary conditions on the surface of the sphere.

Assuming a time dependence of the form $e^{-i\omega t}$, the time-independent elastic wave equation in a homogeneous medium can be written as

$$(\lambda+2\mu)\nabla(\nabla \cdot \mathbf{u}) - \mu\nabla\times\nabla\times\mathbf{u} + \rho\omega^2\mathbf{u} = 0, \qquad (2.1)$$

where $\mathbf{u}$ is the displacement vector, ρ is the mass density and λ, μ are the so-called Lamé coefficients of the medium.[35]

This equation gives rise to uncoupled longitudinal and shear waves with velocities $c_l=\sqrt{(\lambda+2\mu)/\rho}$ and $c_s=\sqrt{\mu/\rho}$, respectively. These waves are mixed through the scattering process.

The solution of (2.1) in spherical coordinates can be reduced to the solution of three scalar Helmholtz equations (see Straton[33]) and has the following general form:

$$\mathbf{u}=\mathbf{l}+\mathbf{m}+\mathbf{n}, \tag{2.2}$$

where $\mathbf{l},\mathbf{m},\mathbf{n}$ are three independent vector solutions of (2.1). Each of them is obtained as a linear combination of vectors $\mathbf{l}^{e}_{o\,nm}$, $\mathbf{m}^{e}_{o\,nm}$, $\mathbf{n}^{e}_{o\,nm}$ (see Appendix A) each one of which comes from a solution of the scalar Helmholtz equation (see Straton[33]).

In the following discussion the subscript "o" (out) in the velocities (c), wave vectors (k), and Z's (see below) is referred to the medium of the matrix and the subscript "i" (in) to the medium of the scatterer. In the vector spherical harmonics $\mathbf{l}$, $\mathbf{m}$, $\mathbf{n}$, and the constants which appeared in the formulas for the cross sections ($A,B\ldots$) the subscripts "e," "o" mean even and odd, respectively (note the double use of "o").

In case (a) we consider a plane longitudinal incident wave of the form:

$$\mathbf{u}^{\mathrm{inc}}(\mathbf{r})=e^{i(\mathbf{k}_{lo}\mathbf{r})}\hat{\mathbf{z}}, \quad k_{lo}=\omega/c_{lo}, \tag{2.3}$$

propagating in the $\hat{\mathbf{z}}$ direction ($\mathbf{k}_{lo}=k_{lo}\hat{\mathbf{z}}$).

This involves the $m=0$, even $\mathbf{l}$ components only and can be written as

$$\mathbf{u}^{\mathrm{inc}}=\sum_{n=0}^{\infty}(-i^{n+1})(2n+1)\mathbf{l}_{en0}(j,k_{lo}). \tag{2.4}$$

The scattered wave and the wave inside the sphere result from the solution of (2.1) in each region and the boundary conditions on the surface of the sphere (see Appendix A) and have the form

$$\mathbf{u}^{\mathrm{sc}}=\sum_{n=0}^{\infty}i^{n}(2n+1)[A_{en0}\mathbf{l}_{en0}(h,k_{lo})+C_{en0}\mathbf{n}_{en0}(h,k_{so})] \tag{2.5}$$

and

$$\mathbf{u}^{\mathrm{in}}=\sum_{n=0}^{\infty}i^{n}(2n+1)[E_{en0}\mathbf{l}_{en0}(j,k_{li})+G_{en0}\mathbf{n}_{en0}(j,k_{si})]. \tag{2.6}$$

The coefficients A_{en0},C_{en0}, are determined in Appendix B. The symbols in the parentheses of $\mathbf{l}$, $\mathbf{n}$ (or $\mathbf{m}$) denote the kind of Bessel function the first, and the wave vector the second which are contained in the definition of $\mathbf{l}$, $\mathbf{n}$ (or $\mathbf{m}$); h is the spherical Hankel function of the first kind, j is the spherical Bessel function, and $k_{so}=\omega/c_{so}$, $k_{li}=\omega/c_{li}$, $k_{si}=\omega/c_{si}$.

The dimensionless scattering cross section ($\hat{\sigma}_l$) for the case of Eq. (2.3) is given by

$$\hat{\sigma}_l=\frac{\sigma_l}{\pi a^2}=\sum_{n=0}^{\infty}4(2n+1)\left[\frac{|A_{en0}|^2}{|Z_{lo}|^2}+n(n+1)\left(\frac{Z_{lo}}{Z_{so}}\right)\frac{|C_{en0}|^2}{|Z_{so}|^2}\right]=\sum_{n=0}^{\infty}\frac{\sigma_l(n)}{\pi a^2} \tag{2.7}$$

where a is the radius of the sphere, $Z_{lo}=k_{lo}a$, and $Z_{so}=k_{so}a=(\omega/c_{so})a$. $\sigma_l(n)$ are the partial scattering cross sections for each mode (n). Each of them, as can be seen from the above formula, is a sum of two terms; the first arises from the longitudinal and the second from the shear scattered wave. For the derivation of $\hat{\sigma}_l$ see Appendix A.

In case (b) we consider a shear $\hat{\mathbf{x}}$-polarized incident wave of the form

$$\mathbf{u}^{\mathrm{inc}}(\mathbf{r})=e^{i(\mathbf{k}_{so}\mathbf{r})}\hat{\mathbf{x}}=\sum_{n=1}^{\infty}i^{n}\frac{2n+1}{n(n+1)}[\mathbf{m}_{on1}(j,k_{so})-i\mathbf{n}_{en1}(j,k_{so})] \tag{2.8}$$

propagating in the $\hat{\mathbf{z}}$ direction ($\mathbf{k}_{so}=k_{so}\hat{\mathbf{z}}$).

In this case the scattered wave is

$$\mathbf{u}^{\mathrm{sc}}=\sum_{n=1}^{\infty}i^{n}\frac{2n+1}{n(n+1)}[A_{en1}\mathbf{l}_{en1}(h,k_{lo})+B_{on1}\mathbf{m}_{on1}(h,k_{so})+C_{en1}\mathbf{n}_{en1}(h,k_{so})], \tag{2.9}$$

the wave inside the sphere is

$$\mathbf{u}^{\mathrm{in}}=\sum_{n=1}^{\infty}i^{n}\frac{2n+1}{n(n+1)}[E_{en1}\mathbf{l}_{en1}(j,k_{li})+F_{on1}\mathbf{m}_{on1}(j,k_{si})+G_{en1}\mathbf{n}_{en1}(j,k_{si})], \tag{2.10}$$

and the dimensionless S scattering cross section ($\hat{\sigma}_s$) is given by (see Appendix A)

$$\hat{\sigma}_s=\frac{\sigma_s}{\pi a^2}=\sum_{n=1}^{\infty}2(2n+1)\left[\frac{1}{n(n+1)}\left(\frac{Z_{so}}{Z_{lo}}\right)\frac{|A_{en1}|^2}{|Z_{lo}|^2}+\frac{|B_{on1}|^2}{|Z_{so}|^2}+\frac{|C_{en1}|^2}{|Z_{so}|^2}\right]=\sum_{n=1}^{\infty}\frac{\sigma_s(n)}{\pi a^2}. \tag{2.11}$$

A_{en1},B_{on1},C_{en1}, are also determined in Appendix B. In the case of S scattering, each partial cross section ($\sigma_s(n)$) is a sum of three terms. The first one is the contribution of the longitudinal scattered wave and the second and third the contribution of the transverse $\mathbf{m}$ and $\mathbf{n}$ scattered waves, respectively.

The infinite sums appearing in the definition of $\hat{\sigma}_l,\hat{\sigma}_s$, in all of our calculations have been approximated with finite sums (by using a truncation criterion) containing, at most, 15 terms. For small frequencies ($Z_l,Z_s<1$), in most of the cases, three or four terms are able to give satisfactory accuracy. In all cases the relative truncation error is less than 10^{-4}.

III. RESULTS AND DISCUSSION

As was mentioned earlier, a systematic examination of the elastic wave propagation through various periodic lattices

consisting of scatterers periodically embedded in a homogeneous matrix — with emphasis in the case of spherical scatterers — has been done and the optimal conditions for gap creation have been extensively studied.[15–20,34]

Here, we try to connect the appearance of a gap and other characteristics of the band structure in a periodic system consisting of spherical inclusions in an homogeneous matrix with the form of the cross section from a single-inclusion. This connection determines to what extent single-sphere scattering is an important factor in determining some characteristic features in the band structure and how it can be used to predict the possible existence of gaps.

For this reason we calculated the cross section from a single scatterer and examined its dependence on

(i) the velocity contrast of the two materials (sphere and matrix),

(ii) the ratio of longitudinal to shear wave velocity in each of them,

(iii) the density contrast of the two materials for both the liquid and the solid case.

We compared this dependence with the aforementioned dependence of some features of the band structure on the same parameters and we connected the position of the resonances with flat bands and possibly with gap positions.

The central idea is to check whether the approach of linear combination of atomiclike orbitals (LCAO or tight-binding method), which is so fruitful for analyzing the electronic band structure in crystalline solids, can be extended to the case of CW propagating in periodic composite media. Cross-section resonances in the CW case are expected to be the analogs of the atomiclike orbitals in the electronic case.

In attempting this extension of the LCAO approach to CW, one should keep in mind some important differences between the two cases: (i) Resonances are not true eigenstates, rigorously localized inside and around each scatterer as the atomiclike orbitals; actually, as will be discussed later on, there are some broad "resonances" associated with a *depletion* of energy distribution within the scattering sphere. (ii) Because of the vector character of EL waves there is much higher degeneracy or near degeneracy than in the electronic case (e.g., the $n=1$ resonant modes corresponding to the three p orbitals in the electronic case are now in general nine); as a result the problem of possible hybridization of the resonances is much more complicated in the EL wave case. (iii) Because ω^2 corresponds to the case where the electronic energy is higher than the maximum of the potential, there is an additional (besides the hopping from resonances of one sphere to resonances of neighboring spheres) mode of propagation employing mainly (or at least on equal basis) the host material. It means that resonant states for CW are states embedded in the continuum; this is an aspect of the problem not encountered in the electronic case. (iv) Another aspect of the EL (and AC) case is associated with the role of the mass density contrast between host and scatterer which seems to be as equally important as the velocity contrast.

In Fig. 1 we show the dimensionless total scattering cross sections $\hat{\sigma}_l$ (a) and $\hat{\sigma}_s$ (b) for longitudinal and shear incident wave, respectively, (L and S scattering). The parameters are as follows: $\rho_o/\rho_i=1$, $c_l/c_s=\sqrt{2}$ ("extreme" solids both in and out) and $c_{lo}/c_{li}=5.48$. The number next to or above

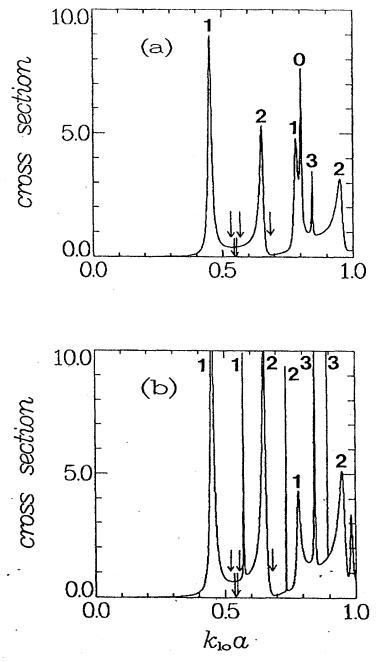

FIG. 1. Total dimensionless cross section vs $k_{lo}a$ for longitudinal (a) and shear (b) incident wave; $c_l/c_s=\sqrt{2}$ for both sphere (in) and matrix (out), $\rho_o/\rho_i=1$ and $c_{lo}/c_{li}=5.48$. a is the radius of the sphere and $k_{lo}=\omega/c_{lo}$ the longitudinal wave number in the medium of the matrix. The number next or above each resonance denotes the spherical harmonic responsible for this resonance. The height of the very narrow resonances may be larger than indicated. The arrows indicate the positions of the flat bands and the double arrow the position of the gap in the corresponding fcc periodic composite with volume fraction of the spheres $x=0.144$.

each resonance denotes the partial wave, the scattering of which causes the appearance of the corresponding resonance (note that in the shear incident wave the $n=0$ mode does not exist). The height of the very narrow resonances (presented as a single vertical line) may be larger than shown in the figures throughout the present work, because our finite mesh points do not always coincide with the maximum for such sharp peaks.

In the case of Fig. 1 the first resonance (appearing in $k_{lo}a=0.45$) arises from the $n=1$ mode. We found that this happens in all cases of materials with small c_l/c_s ratio which we have examined. Another common characteristic of these materials ("hard" solids) is that the higher contribution in all resonances is due to the shear scattered wave.

It is also noticeable that in Fig. 1 and in all other cases examined, the position of the resonances in the L scattering case (with the exception of the $n=0$ resonances) coincides with the position of the **l** and **n** resonances in the S scattering. See, for example, that the first and third resonance in Fig. 1(b), which are both due to the **l** and **n** scattered waves, coincide in position with the first and second (at $k_{lo}a=0.65$) resonance, respectively, of Fig. 1(a). In the S scattering, there are additional, in most of the cases very narrow peaks, corresponding to the **m** scattered wave; see the

second (at $k_{lo}a=0.57$), fourth, and seventh resonances in Fig. 1(b). We shall comment on these sharp resonances later on.

The matrix-spherical inclusions combination shown in Fig. 1 has been studied[18] for various periodic lattice structures: sc with inclusion volume fraction $x=0.144$, bcc with $x=0.144$, fcc with $x=0.144$, and simple hexagonal with $c/a'=3/4$ and $x=0.144$ (a' is the lattice constant to be distinguished from the sphere radius a used throughout in the present work). In all these cases a narrow gap appears at midgap frequency ω_g such that $k_{glo}a=\omega_g a/c_{lo}\approx 0.54$ for all lattices. The position of the midgap frequency is denoted by a double arrow in Fig. 1. Furthermore, the EL wave band structure exhibits[18] flat bands corresponding to rather sharp peaks in the density of states; their positions are denoted by single arrows in Fig. 1. It must be stressed that these flat bands appear at $k_{lo}a=\omega a/c_{lo}\approx 0.52\pm 0.01$, 0.54 ± 0.01, and 0.66 ± 0.01, *independently* of the lattice structure. This strongly suggests that the positions of the flat bands are not influenced appreciably by multiple scattering and are mainly dependent on the single-scattering resonances. Indeed, this seems to be the case as evidenced by the close correlation of the arrows with the resonances in the scattering cross sections. It is worthwhile to note that the first flat band is above the first resonance (by a non-negligible margin), while the second is just below the second resonance [Fig. 1(b)]; the third flat band is again above the third resonance (although the margin is now smaller). The gap lies between the first and the second resonance. Let us mention that one should not expect an exact coincidence between flat bands and resonances because of "level" repulsion and hybridization.

As was noticed above in the S scattering, there are some extremely sharp peaks in the cross section [see Fig. 1(b)]. Sharp peaks correspond to very long lifetimes, i.e., extremely low radiation which in turn means a very weak scattering field (relative to the field inside the sphere). On the basis of this argument, to be substantiated later on, one expects that very sharp peaks in the single-scattering cross section may not appreciably influence the band structure.

In Fig. 2 we plot the total cross section for an incident longitudinal wave and for a gold sphere in a silicon matrix (a) or a lead sphere in a silicon matrix (b) or a lead sphere in beryllium matrix (c). The cross sections for the shear incident wave are shown in Fig. 3.

The general features of these cross sections follow what have been mentioned in the description of Fig. 1 (see, for example, the extra narrow peaks in the S scattering cross section). Also, here, next to or above each resonance appear, in some cases, more than one index. This denotes a coincidence in the resonances of two or more modes.

The band structure of all combinations of Figs. 2,3 for a fcc lattice (with the volume fraction of the spheres being just below 10%) has been calculated[19] and the results for the flat bands (arrows) and the gap (double arrow) are indicated in these figures (Figs. 2,3). Again we observe a correlation between the resonances and the flat bands, although a flat band in the Pb/Be combination [Fig. 2(c), 3(c)] appearing in the middle of the gap does not seem to be related with a resonance.

In all cases shown in Figs. 2 and 3 the first flat band is located above the first resonance and the second below the

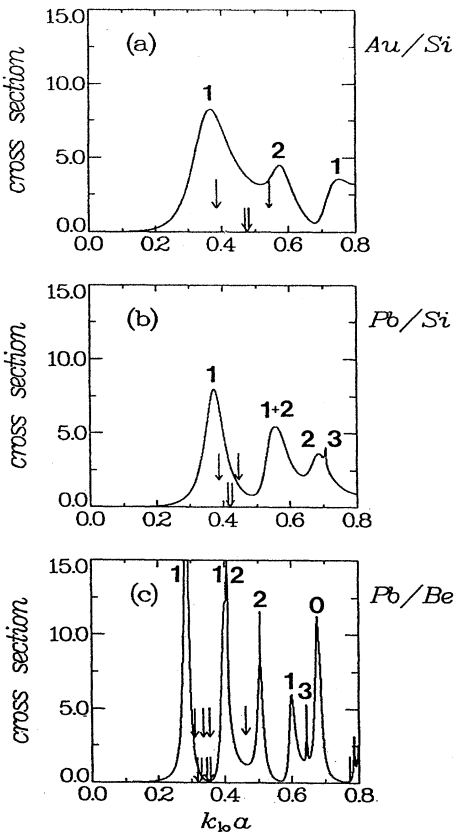

FIG. 2. Total dimensionless cross section vs $k_{lo}a$ for Au spheres in Si matrix (a), Pb spheres in Si matrix (b), and Pb spheres in Be matrix (c). The incident wave is longitudinal; a is the radius of the sphere and $k_{lo}=\omega/c_{lo}$ is the longitudinal wave number in the medium of the matrix. The numbers have the same meaning as in Fig. 1; the arrows indicate the positions of the flat bands and the double arrow the position of the gap in the corresponding fcc periodic composites with volume fraction of the spheres 10% for (a), 9.8% for (b) and 8.23% for (c).

second resonance (if we ignore the sharp resonances appearing in the shear case). The gap lies between the first and the second resonance.

In Fig. 4 we plot the trajectory of the first few flat bands and the two midgaps vs volume fraction of the spheres for an fcc lattice consisting of lead spheres ($\rho=11.357$ g/cm^3, $c_l=2.158$ km/s, $c_s=0.860$ km/s) embedded in epoxy ($\rho=1.180$ g/cm^3, $c_l=2.540$ km/s, $c_s=1.160$ km/s); in the same picture we indicate the position of the first four resonances. We see that the dependence on the volume fraction x occupied by the spheres is weak for $0.2\leq x\leq 0.5$ with a downwards tendency for smaller values of x. For very small values of x the gap disappears while the flat bands tend to coincide with the resonances. The weak dependence on x at intermediate volume fractions is an indication that the multiple scattering is not so important in determining the midgap frequency and the flat bands. The downwards tendency for small x and finally the disappearance of the gap is the same with what has been observed for scalar waves.[26] This downwards tendency is expected because at very low concentra-

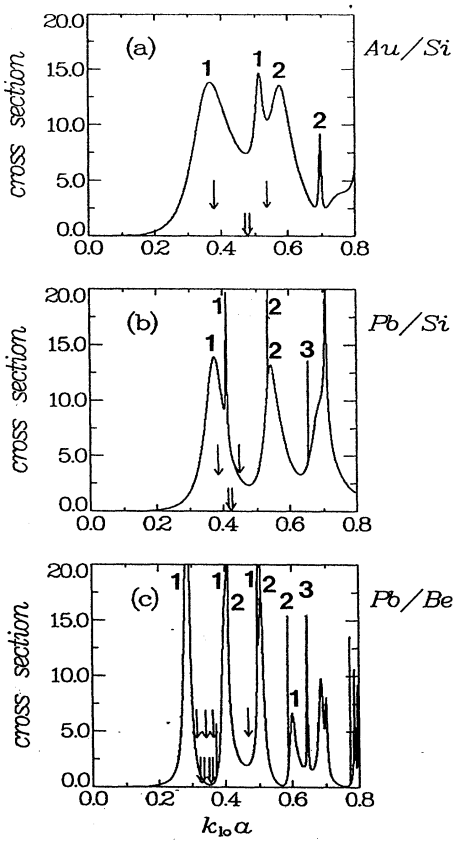

FIG. 3. Total dimensionless cross section vs $k_{lo}a$ for the cases of Fig. 2 but with shear incident wave.

tions the wave propagates mainly through the host and the spheres just obstruct its propagation. As the concentration increases, the resonances can be mixed, broaden into bands and become the preferable channels of propagation at least at certain frequency regions. Thus the gaps tend to be opened near a resonant mode (area of strong individual scattering) at very low concentration of scatterers and move away from it as the concentration increases and the resonances offer themselves for the propagation.

In Figs. 5 and 6 we plot the cross sections for a steel sphere ($\rho=7.8$ g/cm^3, $c_l=5.94$ km/s, $c_s=3.22$ km/s) in an epoxy matrix and vice versa. For the case of a steel sphere in epoxy there is some experimental evidence[17] of spectral gaps; also recent preliminary theoretical results[36] indicate wide gaps. The cross sections for a steel sphere in epoxy are shown in Fig. 5 [panels (a) for longitudinal and (a′) for shear incident wave]. We see that the resonances appear weak buried in a strong background.

Following the analysis of Refs. 30–32 we calculate the scattering cross sections for a rigid sphere in a place of the steel sphere [Figs. 5(b), 5(b′)]. A rigid sphere is one for which $\rho_i\to\infty$, $\mu_i\to\infty$, $\lambda_i\to\infty$, $c_{li}\to 0$, $c_{si}\to 0$, so that the displacement field inside and at the surface of the sphere is zero.

In Figs. 5(c), 5(c′) we plot the cross sections calculated by subtracting from the steel scattering amplitudes the rigid-sphere scattering amplitudes. Then the background disappears (except at very low frequencies) and the two widely separated resonances emerge very clearly [in Fig. 5(c′) the lowest resonance is a double one]. Figure 5 suggests that in the spectral regions where the cross sections of the steel sphere and the rigid sphere are almost identical (e.g., $1.5\leq k_{lo}a\leq 2.5$), the field will hardly penetrate inside the steel sphere.

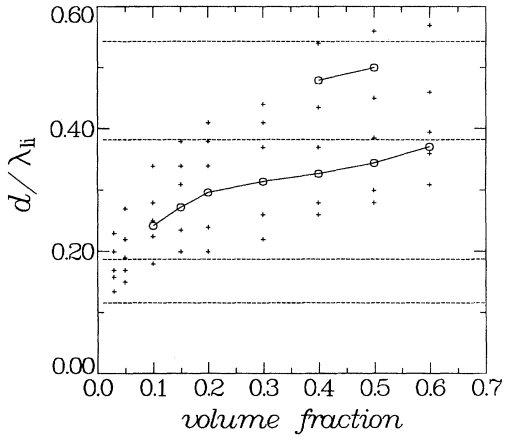

FIG. 4. Midgap frequency (open circles) and "flat" band position (crosses) vs volume fraction of the scatterers for lead spheres in epoxy matrix and fcc structure. "Flat" bands correspond to peaks in the density of states (which may occasionally merge together or become ill-defined). d is the diameter of the sphere ($d=2a$) and $\lambda_{li}=2\pi/k_{li}$ the longitudinal wavelength in the medium of the sphere. The dashed horizontal lines correspond to the first four single-sphere resonances.

We had verified this point by calculating the total field energy density (averaged over the angles) vs r (the distance from the center of the steel sphere); see the dotted line in Fig. 7 corresponding to $k_{lo}a=1.6$. This exclusion of the field from the interior of the sphere implies that in the periodic composite (steel spheres in epoxy) and for these spectral regions (e.g., $1.5\leq k_{lo}a\leq 2.5$) the propagation, if any, must take place almost exclusively through the matrix material (epoxy); this, combined with the large cross section (more than twice the geometrical cross section) strongly suggests that a gap may appear.

Indeed, preliminary results[36] show a rather wide gap [see Fig. 5(c)] surrounded by flat bands as indicated by arrows in Fig. 5(c). These flat bands may be associated with hopping propagation (linear combination of resonance "orbitals") from one steel sphere to its neighbors using the resonances (linear combination of resonance "orbitals").

This picture is also supported by the results shown in Fig. 7, where the solid line corresponds with $k_{lo}a=0.31$ (i.e., the maximum of the rather broad first peak in Fig. 5) and the dashed line to $k_{lo}a=0.867$ (i.e., to the sharp first peak in Fig. 6). We see that the resonances correspond to a field distribution strongly localized inside the sphere (the sharper the peak, the stronger the localization) with some weak leakage outside (the sharper the peak, the weaker the leakage and the less probable the hopping propagation).

From Fig. 7 one can obtain a *rough* estimate of the optimum volume fraction for a wide gap: the neighboring

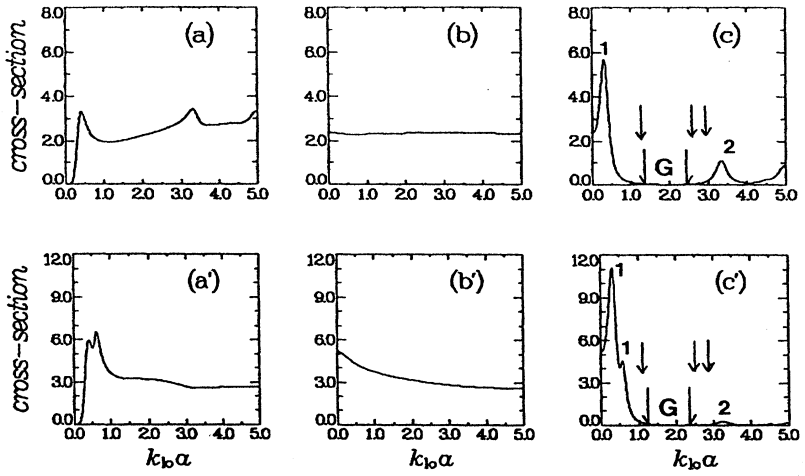

FIG. 5. Total dimensionless cross sections vs $k_{lo}a$ for steel sphere in epoxy matrix (a, a'), rigid sphere in epoxy matrix (b, b'). The third column (c, c') represents the cross section calculated by subtracting from the steel sphere scattering amplitudes the rigid sphere scattering amplitudes. The upper panels correspond to longitudinal incident wave and the lower to shear incident wave. a is the radius of the sphere and $k_{lo}=\omega/c_{lo}$ the longitudinal wave number in the medium of the matrix. The arrows indicate the positions of the flat bands and the double arrow (with the symbol G inside) the position of the gap in the corresponding fcc periodic composite with volume fraction of the spheres $x=0.4524$. The numbers have the same meaning as in Fig. 1.

spheres must be close enough to overlap with the broad maximum of the dotted line (as to make the propagation through the matrix material more difficult) and far apart to avoid the strong broadening of the resonance-based bands. Keeping the neighboring spheres apart by a distance equal to $0.5a$ to a seems to be a reasonable compromise on the basis of Fig. 7. This implies an optimum volume fraction between 37.9% and 21.9% (assuming a close-packed type of lattice).

In Fig. 6 we show the results of the same analysis for the case of an epoxy sphere in a steel matrix. In this case instead of a rigid sphere, the background {which was calculated [Figs 6(b), 6(b')] and subtracted [Figs. 6(c), 6(c')]} refers to a "soft" sphere, defined by $\rho_i\to 0$, $\mu_i\to 0$, $\lambda_i\to 0$, $c_{li}\to 0$, $c_{si}\to 0$. With the subtraction of the background the many sharp resonances (characteristic of the large c_{lo}/c_{li} ratio) emerge very clearly.

On the basis of the arguments developed in connection with Fig. 5, one expects that the periodic composite, epoxy spheres in a steel matrix, is not favorable for producing a wide gap because of the many closely spaced resonances, which would probably produce overlapping bands. The best chance is for a narrow band around $k_{lo}a\approx 1$. Even that is doubtful, because the background cross section around $k_{lo}a$ is not as large as in the case of Fig. 5.

In Fig. 8 we show the effect of the velocity contrast on the cross section for the shear incident wave and for a case where $\rho_o/\rho_i=1/4$, $c_{lo}/c_{so}=c_{li}/c_{si}=\sqrt{2}$ ("extreme" solid). In Fig. 8(a) the velocity ratio $c_{lo}/c_{li}=4$. The low velocity scatterer produces as many sharp resonances in the present elastic case as in the electromagnetic and scalar cases. These sharp resonances disappear when $c_{lo}/c_{li}=1$ [Fig. 8(b)] or when $c_{lo}/c_{li}=1/4$ [Fig. 8(c)]. For a longitudinal incident wave the cross section is smaller, smoother, and with fewer peaks (in agreement with what has been noticed above). The rigid-sphere background (not shown here) is almost constant and large [about four (three) times the geometrical cross section for a shear (longitudinal) incident wave] but does not dominate the cross section at any spectral region. No results for the corresponding periodic case are available. On the basis of the analysis developed in the present work one would guess that there is a small chance for a narrow gap between the first and second (or possibly between the second and third) peak of Fig. 8(a).

In Fig. 9 we show the effects on the longitudinal incident

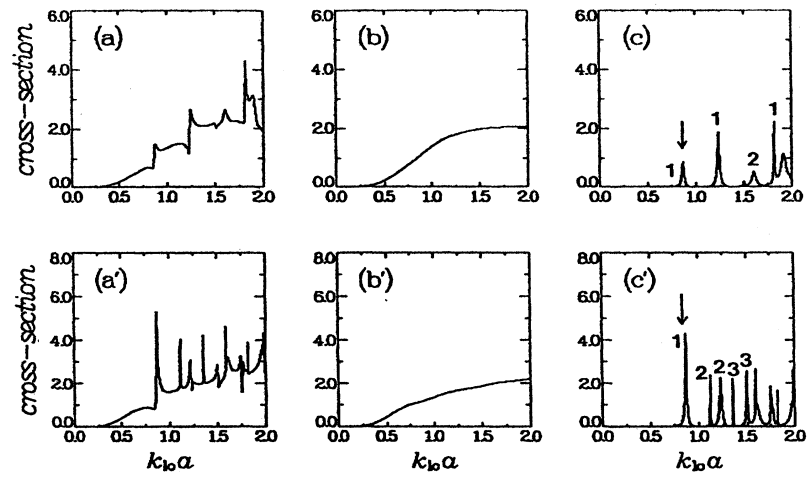

FIG. 6. Total dimensionless cross section vs $k_{lo}a$ for the case of epoxy sphere in steel matrix (a, a'). The upper panels correspond to longitudinal incident wave and the lower to shear incident wave. The second column (b, b') represents the soft sphere in steel matrix cross section and the third (c, c') the cross section calculated by subtracting from the epoxy sphere scattering amplitudes the soft sphere scattering amplitudes. a is the radius of the sphere and $k_{lo}=\omega/c_{lo}$ the longitudinal wave number in the medium of the matrix. The numbers have the same meaning as in Fig. 1 and the arrows indicate the positions of the flat bands in the corresponding sc periodic composite with volume fraction of the spheres $x=0.268$.

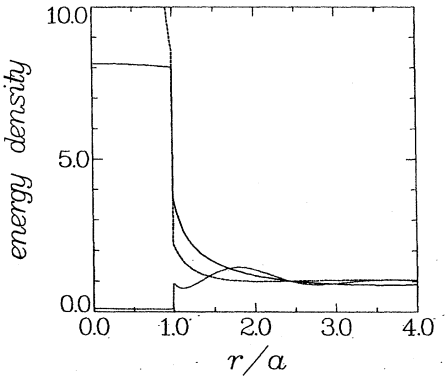

FIG. 7. Total energy density vs r (the distance from the center of the sphere) on a "wide" resonance [first resonance of Fig. 5(c), solid line], on a "narrow" resonance [first resonance of Fig. 6(c), dashed line] and "off" resonance [between the two resonances in Fig. 5(c), dotted line]. The energy is in the incident wave energy density units and the r in units of the sphere radius (a).

wave cross section of increasing the ratio of the longitudinal to shear velocity for the case presented in Fig. 1(a). For the upper panels the ratio $c_l/c_s=2$ and for the lower panels the ratio $c_l/c_s=2.83$.

The background cross sections [panels (b) and (b′)] refer to a soft sphere. For the shear incident wave the picture is more complicated with many additional peaks.

Figure 9 shows that these combinations are not favorable for a spectral gap, because the separation between the first two peaks is not large and the value of the background in between is not so large. Comparing Fig. 1(a) and Figs. 9(a), 9(a′), we see that by increasing the ratio c_l/c_s (in both matrix and sphere) the separation of the first two peaks is reduced making it more and more difficult for a gap to appear. The actual calculation[18] verifies this "educated" guess: indeed the narrow gap of the case in Fig. 1(a) disappears in the cases of Figs. 9(a) and 9(a′) because of the overlap of the first and second flat bands [their midfrequencies are indicated by arrows in Figs. 9(a) and 9(a′)]. Note that the first two flat bands in the cases of Figs. 9(a) and 9(a′) conform with the general picture discussed earlier, i.e., they are located above and below the first and the second resonance, respectively.

In Figs. 10–15 we show results concerning the role of the mass density contrast and its opposite effect on solid and fluid periodic media which constitutes a puzzling and unresolved issue. In Figs. 10 (longitudinal incident wave) and 11 (shear incident wave) we examine a case for which $c_l/c_s=\sqrt{2}$ for both the sphere and the matrix, $c_{lo}/c_{li}=8.66$ and for which $\rho_o/\rho_i=1/4$ [Figs. 10(a), 11(a)], $\rho_o/\rho_i=1$ [Figs. 10(b), 11(b)], and $\rho_o/\rho_i=4$ [Figs. 10(c), 11(c)].

The periodic problem (with volume fraction $x=0.144$ and fcc lattice) has been already studied; the "flat" bands (arrows) and the gap (double arrow) are indicated in Fig. 10. The main feature of the increase of the density ratio ρ_o/ρ_i is that the peaks become narrower (sometimes to the point of disappearance) without their maximum value becoming lower.

Taking into account that the cross section between peaks

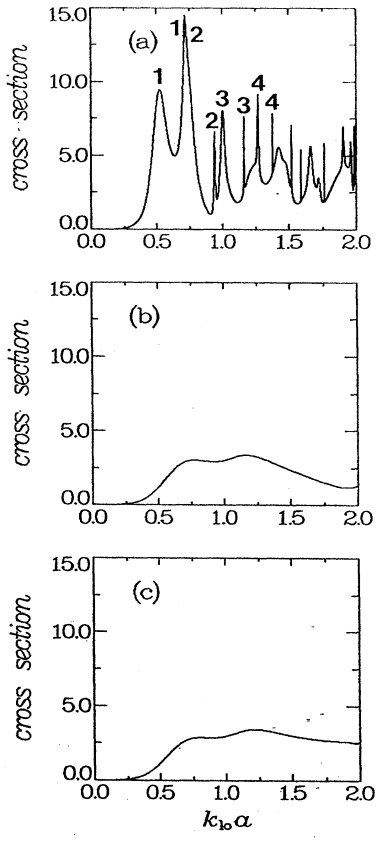

FIG. 8. Total dimensionless cross section vs $k_{lo}a$ for $c_l/c_s=\sqrt{2}$ (for both sphere and matrix), $\rho_o/\rho_i=1/4$ and $c_{lo}/c_{li}=4$ (a), 1 (b), 1/4 (c). The incident wave is shear; a is the sphere radius and $k_{lo}=\omega/c_{lo}$. The numbers next or above each resonance denote its origin (the corresponding modes).

is very small, the reduction of the strength of the peaks with increasing ρ_o/ρ_i implies easier propagation and the eventual disappearance of any gaps in agreement with the actual results.

In Fig. 12 we show results for the total cross section of the corresponding $c_{lo}/c_{li}=8.66$ fluid ($c_s=0$ in both the sphere and the matrix) case with $\rho_o/\rho_i=1/4$, 1, 4 for panels (a), (b), and (c), respectively (note the change of the vertical scale).

What distinguishes the fluid from the solid case is the dominant role of the isotropic oscillation ($n=0$) component. In the solid case the $n=0$ component makes a relatively insignificant contribution at high frequency and for the longitudinal component only (see Fig. 10). On the other hand, for the fluid case the $n=0$ component dominates the background and produces a strong first resonance. This resonance can be studied analytically (see Appendix C) and in the high ρ_o/ρ_i limit the resonance frequency is given by $\omega_o=(c_i/a)\sqrt{3\rho_i/\rho_o}$. Both the background and the first resonance, in contrast to the solid case, become larger as the ratio ρ_o/ρ_i increases (see Fig. 13). This basic difference is shown in Fig. 14 where in panel (a) the area under the first $n=0$ resonance of the fluid case is plotted vs ρ_o/ρ_i, while in panel (b) the areas under the lowest ($n=1$) resonance for

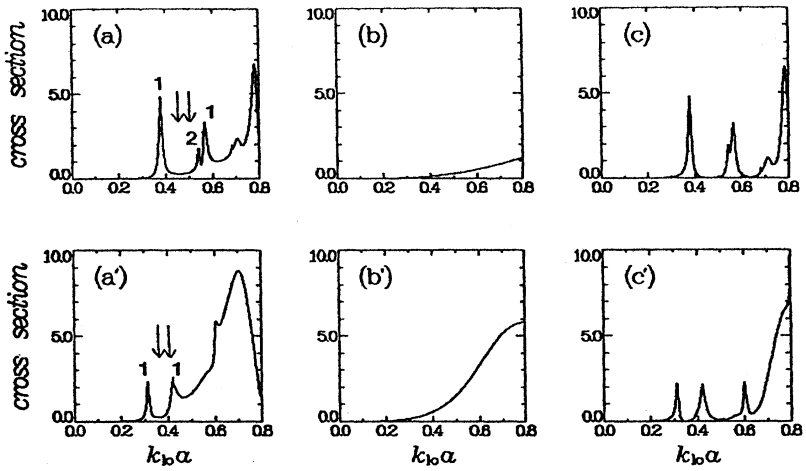

FIG. 9. Total dimensionless cross section vs $k_{lo}a$ for $c_{lo}/c_{li}=5.48$, $\rho_o/\rho_i=1$ and $c_l/c_s=2$ (a), and 2.88 (a′) (for both sphere and matrix). The incident wave is longitudinal. In the second column (b, b′) the above sphere has been replaced by a soft sphere and in the third (c, c′) the cross section was calculated by a subtraction similar to what described Fig. 5. a is the radius of the sphere and $k_{lo}=\omega/c_{lo}$ the longitudinal wave number in the medium of the matrix. The numbers and the arrows have the same meaning as in Fig. 1.

longitudinal (solid line) and shear (dashed line) incident wave are exhibited. The conclusion is that a large density ratio ρ_o/ρ_i is indeed very favorable for gap creation in fluid periodic media because of the $n=0$ component.

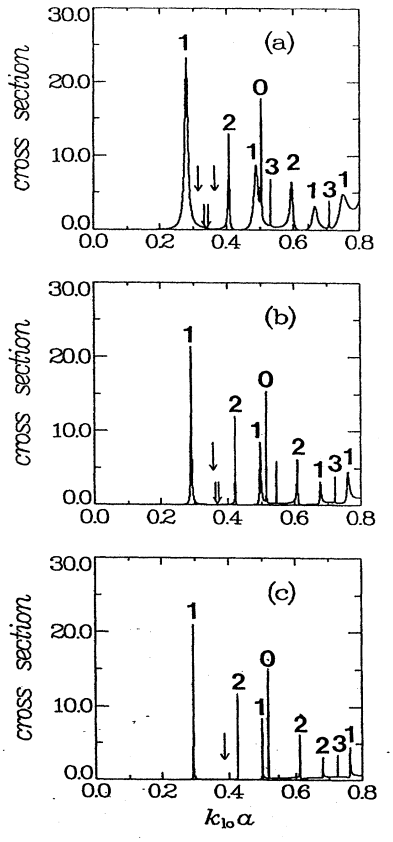

FIG. 10. Total dimensionless cross section vs $k_{lo}a$ for $c_{lo}/c_{li}=8.66$, $c_l/c_s=\sqrt{2}$ for both sphere and matrix and $\rho_o/\rho_i=$ 1/4 (a), 1 (b), 4(c). a is sphere radius and $k_{lo}=\omega/c_{lo}$. The incident wave is longitudinal; the numbers, arrows, and the double arrow have the same meaning as in Fig. 1.

In Fig. 15 we show the cross section for a fluid sphere in a fluid matrix with velocity contrast $c_{lo}/c_{li}=2.65$ and density contrast $\rho_o/\rho_i=1/5$ [panel (a)], 1 [(panel (b)], and 15 [panel (c)]. The corresponding periodic case has been studied before.[15] The case of Fig. 15(a) exhibits no gaps but show sharp peaks in the density of states [arrows in Fig. 15(a)]. The case of Fig. 15(b) develops two gaps: a relatively wide

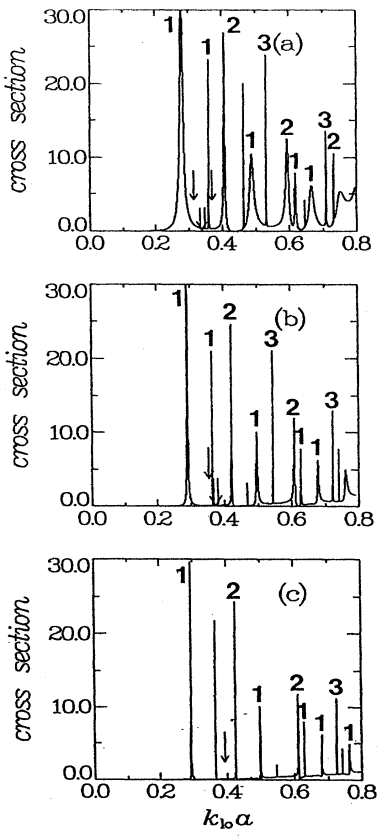

FIG. 11. Total dimensionless cross section vs $k_{lo}a$ for the cases of Fig. 10 and for shear incident wave.

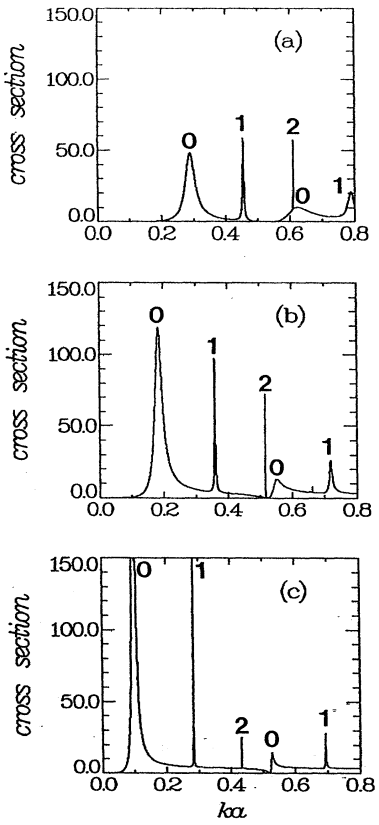

FIG. 12. Dimensionless scattering cross section vs ka for $c_{lo}/c_{li}=8.66$, $c_{so}=c_{si}=0$ (liquid case) and $\rho_o/\rho_i=$ 1/4 (a), 1 (b), 4 (c). a is the radius of the sphere, $k=\omega/c_{lo}$. The number above each resonance indicates the spherical harmonic responsible for the resonance.

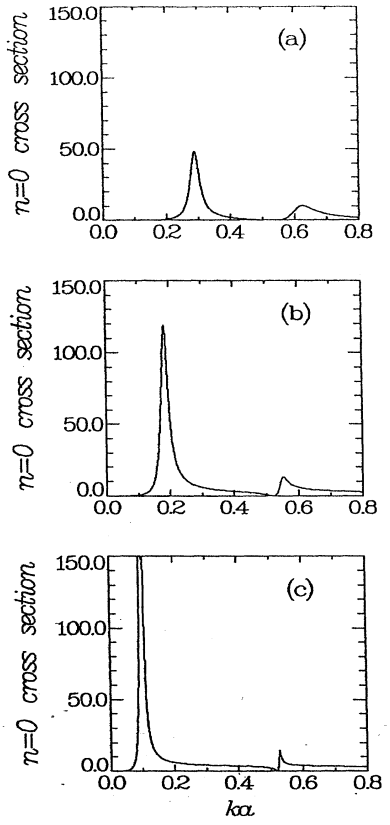

FIG. 13. Dimensionless $n=0$ partial cross section vs ka for the cases of Fig. 12.

one between the first and the second "flat" band (arrows) and a narrow one just above the third "flat" band. The case of Fig. 15(c) has three gaps: a very wide one extending from the first to second arrow, a second one extending from $ka\approx 1.25$ to $ka\approx 1.5$, and a third one above the fourth arrow. Note also the correspondence between the resonances and the "flat" bands with the exception of the second resonance which was expected to produce a flat band in the middle (approximately) of the very wide gap; such a band does not appear in the results of Ref. 15.

The large gaps associated with the case $\rho_o/\rho_i=15$ is again due to the strong scattering (both the low-lying resonance and the background) associated with the isotropic ($n=0$) oscillation.

In view of the above results, it is interesting to examine what happens in the mixed cases of a solid sphere in a fluid host or a fluid sphere in a solid matrix. Preliminary results indicate that the solid sphere in fluid behaves similarly to the fluid in fluid case, while the fluid sphere in solid follows the solid in solid behavior. This is not surprising, since for the $n=0$ mode (which is purely compressional) there is no difference between a solid and a fluid sphere with the same ρ_i and $B_i=\lambda_i+(2/3)\mu_i$.

IV. CONCLUDING REMARKS

We have examined the dependence of the cross sections of an elastic sphere embedded in an infinite homogeneous elastic medium on various parameters such as velocity contrast c_{lo}/c_{li}, mass density contrast, "solidity" of the sphere (c_{li}/c_{si}), and the host (c_{lo}/c_{so}).

We have paid particular attention to the various resonances appearing in the cross section and we have connected them with specific spherical harmonic modes. In many cases it was useful to calculate and subtract the cross section and the scattering amplitude, respectively, corresponding to a rigid or soft sphere. We have connected the above data for the scattering from a single sphere with the features of the band structure associated with the propagation of elastic waves in a periodic medium consisting of spheres embedded in an homogeneous matrix. In particular we were interested in "flat" bands (peaks in the density of states) and spectral gaps. We found that the resonances in the single scattering were closely associated with the "flat" bands supporting thus the idea of a linear combination of resonance states (in analogy with the LCAO approach in the electronic propagation in solids).

In addition to this hopping propagation from sphere to sphere (utilizing the resonances) there is another mode of propagation utilizing mainly the host material. The analysis through the rigid or soft sphere is helpful in deciding whether one of the two modes of propagation (hopping or

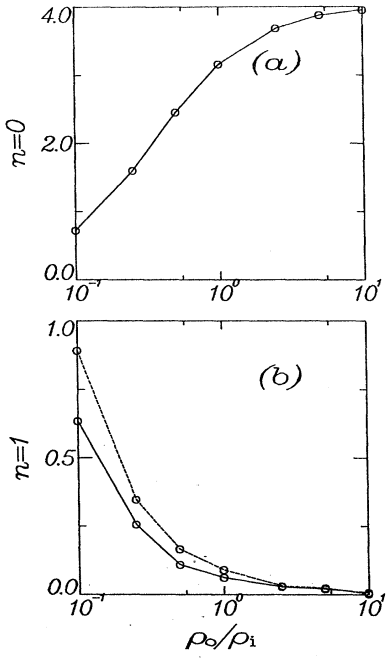

FIG. 14. (a) Area under the dominant $n=0$ first resonance vs ρ_o/ρ_i for $c_l/c_s=10$ for both matrix and sphere (fluidlike case). (b) Area under the dominant $n=1$ first resonance vs ρ_o/ρ_i for $c_l/c_s=\sqrt{2}$ for both matrix and sphere (extreme solid case). The solid line corresponds to longitudinal incident wave and the dashed line to shear incident wave. For both panels $c_{lo}/c_{li}=8.66$.

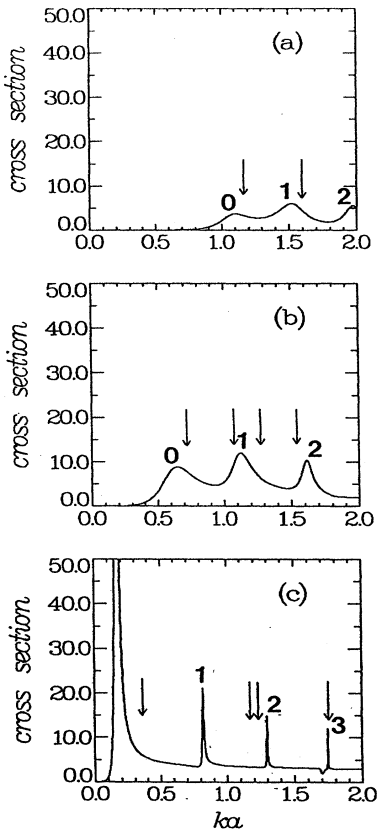

FIG. 15. Dimensionless scattering cross section vs ka for $c_{lo}/c_{li}=2.65, c_{so}=c_{si}=0$ (liquid case) and $\rho_o/\rho_i=$ 1/5 (a), 1 (b), 15 (c). a is the sphere radius and $k=\omega/c_{lo}$. The numbers have the same meaning as in Fig. 1 and the arrows indicate the positions of the peaks in the density of states of the corresponding fcc periodic system with volume fraction of the spheres $x=0.144$.

through the host) is dominant or whether the wave utilizes both the host and the spheres for its propagation.

We have developed some criteria for the appearance of gaps in the periodic case on the basis of the single-sphere scattering, e.g., widely separated resonances (especially the lowest ones) with a strong background in between (due to the rigid or soft sphere) are very favorable for wide gaps and consequently for localized states in a disordered composite medium.

ACKNOWLEDGMENTS

The present work was supported by GSRT-Hellas Grant No. 91EΔ556 and by EU Grants No. SCC-CT90-0020, ERBCHRX-CT93-0136-0331-0332, and MAS2-CT92-0019. We thank M. Sigalas for useful discussions and for providing us with his band-structure computer programs. Useful communications with G. Gaunaurd are also acknowledged.

APPENDIX A

In this appendix, we present the general solution of the elastic wave equation in spherical coordinates, the boundary conditions on the surface of the sphere and the formulas used for the derivation of the scattering cross sections.

The time-dependent elastic wave equation in an homogeneous medium is

$$(\lambda+2\mu)\nabla(\nabla\cdot\mathbf{U})-\mu\nabla\times\nabla\times\mathbf{U}=\rho\frac{\partial^2\mathbf{U}}{\partial t^2}. \quad \text{(A1)}$$

Assuming the time dependence to be of the form $e^{-i\omega t}$, the general solution of (A1) in spherical coordinates (r,θ,ϕ) can be written as

$$\mathbf{U}=e^{-i\omega t}\mathbf{u} \quad \text{(A2)}$$

with

$$\mathbf{u}=\mathbf{l}+\mathbf{m}+\mathbf{n}, \quad \text{(A3)}$$

where

$$\mathbf{l}=\sum_{\substack{e\\o}}\sum_{n,m} Z^{e}_{o\,nm}\,\mathbf{l}^{e}_{o\,nm},\ \mathbf{m}=\sum_{\substack{e\\o}}\sum_{n,m} H^{e}_{o\,nm}\,\mathbf{m}^{e}_{o\,nm},\ \mathbf{n}=\sum_{\substack{e\\o}}\sum_{n,m} \Theta^{e}_{o\,nm}\,\mathbf{n}^{e}_{o\,nm}, \quad \text{(A4)}$$

and

$$\mathbf{l}^{e}_{o\,nm}=\frac{1}{k_l}\frac{\partial}{\partial r}R_n(k_lr)P_n^m(\cos\theta)^{\cos}_{\sin}\,m\phi\,\hat{\mathbf{r}}$$
$$+\frac{1}{k_lr}R_n(k_lr)\frac{\partial}{\partial\theta}P_n^m(\cos\theta)^{\cos}_{\sin}\,m\phi\,\hat{\theta}$$
$$\mp\frac{m}{k_lr\sin\theta}R_n(k_lr)P_n^m(\cos\theta)^{\sin}_{\cos}\,m\phi\,\hat{\phi}, \quad \text{(A5)}$$

$$\mathbf{m}_{o}^{e}{}_{nm} = \mp \frac{m}{\sin\theta} R_n(k_s r) P_n^m(\cos\theta)_{\cos}^{\sin} m\phi\ \hat{\theta} - R_n(k_s r) \frac{\partial}{\partial\theta} P_n^m(\cos\theta)_{\sin}^{\cos} m\phi\ \hat{\phi}, \tag{A6}$$

$$\mathbf{n}_{o}^{e}{}_{nm} = \frac{n(n+1)}{k_s r} R_n(k_s r) P_n^m(\cos\theta)_{\sin}^{\cos} m\phi \hat{\mathbf{r}} + \frac{1}{k_s r}\frac{\partial}{\partial r}[rR_n(k_s r)] \frac{\partial}{\partial\theta} P_n^m(\cos\theta)_{\sin}^{\cos} m\phi\ \hat{\theta} \mp \frac{m}{k_s r \sin\theta}\frac{\partial}{\partial r}[rR_n(k_s r)]\ P_n^m(\cos\theta)_{\cos}^{\sin} m\phi\ \hat{\phi}\ . \tag{A7}$$

$\hat{\mathbf{r}}$ $\hat{\theta}$ $\hat{\phi}$ are the spherical unit vectors; $k_l = \omega/c_l$, $k_s = \omega/c_s$ with ω the frequency, c_l is the longitudinal, and c_s is the shear wave velocity in the medium; $\lambda = \rho(c_l^2 - 2c_s^2)$, $\mu = \rho c_s^2$ are the Lamé coefficients of the medium (ρ is the mass density); R_n is an appropriate Bessel function (chosen from the boundary conditions at $r \to 0$ or $r \to \infty$); P_n^m are the associated Legendre polynomials.

The subscripts "e" and "o" which appear in the definition of $\mathbf{l}_{o}^{e}{}_{nm}$, $\mathbf{m}_{o}^{e}{}_{nm}$, $\mathbf{n}_{o}^{e}{}_{nm}$, and in the coefficients $Z_{o}^{e}{}_{nm}$, $H_{o}^{e}{}_{nm}$, $\Theta_{o}^{e}{}_{nm}$ [see (A4)], mean even and odd, respectively, and the subscripts n and m are integers going from zero to infinity the first and from zero to n the second.

The boundary conditions on the surface of the sphere ($r = a$) which are the continuity of normal and tangential displacements and of normal and tangential stresses, can be expressed as

(a) Continuity of the displacements:

$$u_i^{\text{inc}}|_{r=a} + u_i^{\text{sc}}|_{r=a} = u_i^{\text{in}}|_{r=a}, \quad i:(r,\theta,\phi), \tag{A8}$$

(b) Continuity of the stresses:

$$P_i^{\text{inc}}|_{r=a} + P_i^{\text{sc}}|_{r=a} = P_i^{\text{in}}|_{r=a}, \quad i:(r,\theta,\phi), \tag{A9}$$

where

$$P_i = \sum_j \sigma_{ij} n_j, \quad i,j,l:(r,\theta,\phi), \tag{A10}$$

with n_j the components of the outgoing unit vector normal to the surface of the sphere which in our case is the $\hat{\mathbf{r}}$.

$$\sigma_{ij} = 2\rho c_s^2 u_{ij} + \rho(c_l^2 - 2c_s^2)\delta_{ij}\sum_l u_{ll}, \quad i,j,l:(r,\theta,\phi). \tag{A11}$$

are the stress tensor elements[35] and u_{ij} the strain tensor elements which result from the components of the displacement vector (for the calculation of u_{ij} in the spherical coordinate system, see Ref. 35). The superscripts inc, sc, in, denote the incident, the scattered, and the inner field, respectively.

The *total scattering cross section* for an incident plane wave propagating in the $\hat{\mathbf{z}}$ direction and scattered by a sphere is given by

$$\sigma = \int \frac{j_r^{\text{sc}} r^2}{j_z^{\text{inc}}} d\Omega \quad \text{for} \quad r \to \infty, \tag{A12}$$

where

$$j_i^a = \left\langle \sum_j \text{Re}(\sigma_{ij}^a)\ \text{Re}(\dot{u}_j^a) \right\rangle \tag{A13}$$

$$= \tfrac{1}{2}\omega \sum_j \text{Im}[(\sigma_{ij}^a)^* u_j^a] \quad i,j:(r,\theta,\phi)\ \text{ or }\ i,j:(x,y,z) \qquad a:\text{sc or inc.} \tag{A14}$$

The symbols $\langle\rangle$ denote time average and the Im, (*) and $(\dot{\cdot})$, imaginary part, complex conjugate and time derivative, respectively, while the (A14) is valid only for a wave with time dependence of the form $e^{-i\omega t}$.

APPENDIX B

In this appendix, we present the results from the calculations of the coefficients $A_{en0}, C_{en0}, A_{en1}, B_{on1}, C_{en1}$ which appeared in the formulas for the cross sections [see (2.7) and (2.11)].

We present them for completeness and because of a few misprints which were found in papers where these coefficients are given. Furthermore, here, both the longitudinal and the shear incident wave scattering expressions are given under a single heading — something that could be useful for the interested reader.

The unknown coefficients $A_{en0}, C_{en0}, A_{en1}, B_{on1}, C_{en1}$ (with the subscripts "e" and "o" to mean even and odd, respectively, and the subscript n to go from zero to infinity) are given by

$$A_{en0} = \frac{1}{D_n}\begin{vmatrix} a_{15}^l & a_{12} & a_{13} & a_{14} \\ a_{25}^l & a_{22} & a_{23} & a_{24} \\ a_{35}^l & a_{32} & a_{33} & a_{34} \\ a_{45}^l & a_{42} & a_{43} & a_{44} \end{vmatrix},$$

$$C_{en0} = \frac{1}{D_n}\begin{vmatrix} a_{11} & a_{15}^l & a_{13} & a_{14} \\ a_{21} & a_{25}^l & a_{23} & a_{24} \\ a_{31} & a_{35}^l & a_{33} & a_{34} \\ a_{41} & a_{45}^l & a_{43} & a_{44} \end{vmatrix}, \tag{B1}$$

$$A_{en1} = \frac{1}{D_n}\begin{vmatrix} a_{15}^s & a_{12} & a_{13} & a_{14} \\ a_{25}^s & a_{22} & a_{23} & a_{24} \\ a_{35}^s & a_{32} & a_{33} & a_{34} \\ a_{45}^s & a_{42} & a_{43} & a_{44} \end{vmatrix},$$

$$C_{en1} = \frac{1}{D_n}\begin{vmatrix} a_{11} & a_{15}^s & a_{13} & a_{14} \\ a_{21} & a_{25}^s & a_{23} & a_{24} \\ a_{31} & a_{35}^s & a_{33} & a_{34} \\ a_{41} & a_{45}^s & a_{43} & a_{44} \end{vmatrix}, \tag{B2}$$

$$B_{on1}=[e_{13}e_{22}-e_{23}e_{12}]/[e_{11}e_{22}-e_{21}e_{12}],$$

$$D_n=\begin{vmatrix} a_{11} & a_{12} & a_{13} & a_{14} \\ a_{21} & a_{22} & a_{23} & a_{24} \\ a_{31} & a_{32} & a_{33} & a_{34} \\ a_{41} & a_{42} & a_{43} & a_{44} \end{vmatrix}. \tag{B3}$$

a_{ij}, e_{ij} result from the boundary conditions on the surface of the sphere and have the following form:

$$\begin{aligned} a_{11}&=h_n'(Z_{lo}), \\ a_{12}&=n(n+1)h_n(Z_{so})/Z_{so}, \\ a_{13}&=-j_n'(Z_{li}), \\ a_{14}&=-n(n+1)j_n(Z_{si})/Z_{si}, \\ a_{15}^l&=\iota j_n'(Z_{lo}), \\ a_{15}^s&=\iota n(n+1)j_n(Z_{so})/Z_{so}. \end{aligned} \tag{B4}$$

$$\begin{aligned} a_{21}&=h_n(Z_{lo})/Z_{lo}, \\ a_{22}&=h_n'(Z_{so})+h_n(Z_{so})/Z_{so}, \\ a_{23}&=-j_n(Z_{li})/Z_{li}, \\ a_{24}&=-j_n'(Z_{si})-j_n(Z_{si})/Z_{si}, \\ a_{25}^l&=ij_n(Z_{lo})/Z_{lo}, \\ a_{25}^s&=\iota[j_n'(Z_{so})+j_n(Z_{so})/Z_{so}]. \end{aligned} \tag{B5}$$

$$\begin{aligned} a_{31}&=Z_{lo}[2\mu_o h_n''(Z_{lo})-\lambda_o h_n(Z_{lo})], \\ a_{32}&=2n(n+1)\mu_o[h_n'(Z_{so})-h_n(Z_{so})/Z_{so}], \\ a_{33}&=-Z_{li}[2\mu_i j_n''(j_{li})-\lambda_i j_n(Z_{li})], \\ a_{34}&=-2n(n+1)\mu_i[j_n'(Z_{si})-j_n(Z_{si})/Z_{si}], \\ a_{35}^l&=iZ_{lo}[2\mu_o j_n''(Z_{lo})-\lambda_o j_n(Z_{lo})], \\ a_{35}^s&=2in(n+1)\mu_o[j_n'(Z_{so})-j_n(Z_{so})/Z_{so}]. \end{aligned} \tag{B6}$$

$$\begin{aligned} a_{41}&=2\mu_o[h_n'(Z_{lo})-h_n(Z_{lo})/Z_{lo}], \\ a_{42}&=\mu_o[Z_{so}h_n''(Z_{so})+(n-1)(n+2)h_n(Z_{so})/Z_{so}], \\ a_{43}&=-2\mu_i[j_n'(Z_{li})-j_n(Z_{li})/Z_{li}], \\ a_{44}&=-\mu_i[Z_{si}j_n''(Z_{si})+(n-1)(n+2)j_n(Z_{si})/Z_{si}], \\ a_{45}^l&=2i\mu_o[j_n'(Z_{lo})-j_n(Z_{lo})/Z_{lo}], \\ a_{45}^s&=i\mu_o[Z_{so}j_n''(Z_{so})+(n-1)(n+2)j_n(Z_{so})/Z_{so}], \end{aligned} \tag{B7}$$

$$\begin{aligned} e_{11}&=h_n(Z_{so}), \\ e_{12}&=-j_n(Z_{si}), \\ e_{13}&=-j_n(Z_{so}), \\ e_{21}&=\mu_o Z_{so}[h_n'(Z_{so})-h_n(Z_{so})/Z_{so}], \\ e_{22}&=-\mu_i Z_{si}[j_n'(Z_{si})-j_n(Z_{si})/Z_{si}], \\ e_{23}&=-\mu_o Z_{so}[j_n'(Z_{so})-j_n(Z_{so})/Z_{so}], \end{aligned} \tag{B8}$$

where

$$Z_{l\ell}=k_{l\ell}a=\frac{\omega}{c_{l\ell}}a, \quad Z_{s\ell}=k_{s\ell}a=\frac{\omega}{c_{s\ell}}a,$$

$$\mu_\ell=\rho_\ell c_{s\ell}^2,$$

$$\lambda_\ell=\rho_\ell(c_{l\ell}^2-2c_{s\ell}^2), \quad \ell=o(\text{out}),i(\text{in}).$$

The subscripts "o" (out) and "i" (in), refer to the medium of the matrix and the scatterer, respectively, ρ_ℓ is the mass density, $c_{l\ell}$ and $c_{s\ell}$ are the longitudinal and the shear wave velocity in the medium $\ell(=o,i)$, j_n denotes the spherical Bessel function, and h_n the spherical Hankel function of the first kind ($h_n^{(1)}$). [Note the different meaning of subscript "o" in the definition of B_{on1}. Also note the difference between "i" (in) (used as subscript in this appendix) with $i=\sqrt{-1}$.]

APPENDIX C

In this appendix we will calculate the scattering cross sections for a longitudinal wave, scattered in a liquid sphere embedded in a liquid host. We will derive analytical expressions for some limited cases.

We assume the incident wave displacement field to have the form $\mathbf{U}=e^{-i\omega t}\mathbf{u}$ with $\mathbf{u}=e^{i\mathbf{k}_o\mathbf{r}}\hat{\mathbf{z}}$ and $\mathbf{k}_o=k_o\hat{\mathbf{z}}=\omega/c_o\hat{\mathbf{z}}$. c_o is the wave velocity in the host (out) while with c_i (see below) we denote the wave velocity in the medium of sphere (in). Note the difference between i (in), used as a subscript in this appendix and $i=\sqrt{-1}$.

The incident wave — in terms of spherical waves — can be written as (see Eq. (2.4) and Appendix A)

$$u^{\text{inc}}=\sum_{n=0}^{\infty}(-i^{n+1})(2n+1)\mathbf{l}_{en0}(j,k_o). \tag{C1}$$

The scattered wave and the wave inside the sphere will have the form

$$u^{\text{sc}}=\sum_{n=0}^{\infty} i^n(2n+1)A_{en0}\mathbf{l}_{en0}(h,k_o), \tag{C2}$$

$$u^{\text{in}}=\sum_{n=0}^{\infty} i^n(2n+1)B_{en0}\mathbf{l}_{en0}(j,k_i). \tag{C3}$$

For the definition of $\mathbf{l}_{en0}$ see Appendix A. The symbols in the parentheses of $\mathbf{l}_{en0}$ denote the kind of bessel function and the wave vector which contained in the expressions for the

$\mathbf{l}_{en0}$; $k_o=\omega/c_o$, $k_i=\omega/c_i$ and j, h are the spherical bessel function and the spherical hankel function of the first kind, respectively.

The unknown coefficients A_{en0}, B_{en0} can been determined from the boundary conditions on the surface of the sphere which are the continuity of normal displacements, u_r in this case, and the continuity of normal stresses σ_{rr}.

σ_{rr} can been calculated as described in Appendix A and has the form

$$\sigma_{rr}^{\ell}=-\sum_{n=0}^{\infty}(2n+1)i^n\lambda^{\ell}k^{\ell}D^{\ell}R_n^{\ell}(k^{\ell}r)P_n(\cos\theta). \tag{C4}$$

The superscript ℓ means inc, sc or in. For the incident field $D^{\ell}=-i$, $R_n^{\ell}=j_n$, $k^{\ell}=k_o$, and $\lambda^{\ell}=\rho_o c_o^2$; for the scattered field $D^{\ell}=A_{en0}$, $R_n^{\ell}=h_n$, $k^{\ell}=k_o$, and $\lambda^{\ell}=\rho_o c_o^2$; for the inner field $D^{\ell}=B_{en0}$, $R_n^{\ell}=j_n$, $k^{\ell}=k_i$, and $\lambda^{\ell}=\rho_i c_i^2$ (ρ_o, ρ_i: the mass density out and in, respectively). P_n are the Legendre polynomials.

The application of the boundary conditions on the surface of the sphere ($r=a$) gives for the A_{en0}

$$A_{en0}=i\,\frac{\psi\Delta\; j_n(Z_o)j_n'(Z_i)-j_n(Z_i)j_n'(Z_o)}{\psi\Delta\; h_n(Z_o)j_n'(Z_i)-j_n(Z_i)h_n'(Z_o)}. \tag{C5}$$

$Z_o=k_o a$, $Z_i=k_i a$, $\Delta=\rho_o/\rho_i$ (the density contrast of the two materials) and $\psi=c_o/c_i=Z_i/Z_o$ (the velocity contrast). The dimensionless cross section is given by [see Eq. (2.7)]

$$\hat{\sigma}_l=\frac{\sigma_l}{\pi a^2}=\sum_{n=0}^{\infty}4(2n+1)\frac{|A_{en0}|^2}{|Z_o|^2}. \tag{C6}$$

Taking in to account that $h_n=j_n+iy_n$, we see that $|A_{en0}|\leq 1$; the equality is obtained when

$$\psi\Delta\; y_n(Z_o)j_n'(Z_i)=j_n(Z_i)y_n'(Z_o). \tag{C7}$$

Equation (C7), which can be rewritten as

$$\frac{y_n'(Z_o)}{y_n(Z_o)}=\psi\Delta\frac{j_n'(Z_i)}{j_n(Z_i)}, \tag{C8}$$

is also the condition for a resonance to appear.

We are interested in finding the low-lying resonances for which Z_o, $Z_i\ll 1$. In this case the Bessel functions can be expanded:

$$\frac{y_n'(Z_o)}{y_n(Z_o)}\approx-\frac{n+1}{Z_o}+\frac{n}{1-2n}Z_o,\quad \frac{j_n'(Z_i)}{j_n(Z_i)}\approx\frac{n}{Z_i}-\frac{1}{2n+3}Z_i. \tag{C9}$$

Substituting (C9) in (C8) we see that there is no solution for $n\neq 0$, which means that the lowest $n\neq 0$ resonances do not satisfy the conditions $Z_o, Z_i\ll 1$. For $n=0$, we have from (C9) and (C8):

$$Z_i^2=\frac{3}{\Delta}$$

which is valid only if $\Delta\gg 3$ and $\psi^2\Delta\gg 3$. Under these conditions there is a low-lying resonance at

$$k_i a\approx\sqrt{\frac{3\rho_i}{\rho_o}} \tag{C10}$$

or

$$\omega\approx\frac{c_i}{a}\sqrt{\frac{3\rho_i}{\rho_o}}. \tag{C11}$$

[1] S. John and R. Rangarajan, Phys. Rev. B **38**, 10 101 (1988).
[2] E. N. Economou and A. Zdetsis, Phys. Rev. B **40**, 1334 (1989).
[3] C. M. Soukoulis, E. N. Economou, G. S. Grest, and M. H. Cohen, Phys. Rev. Lett. **62**, 575 (1989).
[4] J. M. Drake and A. Z. Genack, Phys. Rev. Lett. **63**, 259 (1989).
[5] E. Yablonovitch and T. J. Gmitter, Phys. Rev. Lett. **63**, 1950 (1989).
[6] K. M. Ho, C. T. Chan, and C. M. Soukoulis, Phys. Rev. Lett. **65**, 3152 (1990).
[7] K. M. Leung and Y. F. Liu, Phys. Rev. Lett. **65**, 2646 (1990).
[8] Z. Zhang and S. Satpathy, Phys. Rev. Lett. **65**, 2650 (1990).
[9] J. Maddox, Nature (London) **348**, 481 (1990).
[10] P. St. J. Russel, Phys. World **5**, 37 (1992).
[11] *Photonic Band Gaps and Localization*, edited by C. M. Soukoalis (Plenum, New York, 1993).
[12] *Scattering and Localization of Classical Waves in Random Media*, edited by P. Sheng (World Scientific, Singapore, 1990).
[13] P. Sheng, *Introduction to Wave Scattering, Localization and Mesoscopic Phenomena* (Academic, San Diego, 1995).
[14] J. Joannopoulos, R. Meade, and J. Winn, *Photonic Crystals* (Princeton University Press, Princeton, NJ, 1995).
[15] M. M. Sigalas and E. N. Economou, J. Sound Vib. **158**, 377 (1992).
[16] M. M. Sigalas and E. N. Economou, Solid State Commun. **86**, 141 (1993).
[17] V. K. Kinra and E. L. Ker, Int. J. Solids Structures **19**, 393 (1983).
[18] E. N. Economou and M. Sigalas, in *Photonic Band Gaps and Localization*, edited by C. M. Soukoulis (Plenum, New York, 1993), p. 317.
[19] E. N. Economou and M. Sigalas, J. Acoust. Soc. Am. **95**, 1734 (1994).
[20] M. M. Sigalas, E. N. Economou, and M. Kafesaki, Phys. Rev. B **50**, 3393 (1994).
[21] S. John, Phys. Rev. Lett. **53**, 2169 (1983).
[22] P. Sheng and Z. Q. Zhang, Phys. Rev. Lett. **57**, 1879 (1986).
[23] K. M. Ho, C. T. Chan, C. M. Soukoulis, R. Biswas, and M. Sigalas, Solid State Commun. **89**, 413 (1994).
[24] G. Cody, L. Ye, M. Zhou, P. Sheng, and A. N. Norris, *Photonic Band Gaps and Localization* (Ref. 11), p. 339.
[25] See, e.g., J. Acoust. Soc. Am. **93**, 2291 (1993); **93**, 2310 (1993).
[26] S. Datta, C. T. Chan, K. M. Ho, C. M. Soukoulis, and E. N. Economou, in *Photonic Band Gaps and Localization*, edited by C. M. Soukoulis (Plenum, New York, 1993), p. 289.
[27] C. F. Yiang and R. Truell, J. Appl. Phys. **27**, 1086 (1956).
[28] N. Einspruch, E. Witterhold, and R. Truell, J. Appl. Phys. **31**, 806 (1960).

[29] G. Johnson and R. Truell, J. Appl. Phys. **36**, 3467 (1965).
[30] G. Gaunaurd and H. Uberall, J. Acoust. Soc. Am. **67**, 1432 (1980).
[31] G. Gaunaurd and H. Uberall, J. Acoust. Soc. Am. **81**, 1 (1987).
[32] L. Flax, G. Gaunaurd, and H. Uberall, in *Physical Acoustics*, edited by W. P. Mason (Academic, New York, 1981), Vol. XV.
[33] J. A. Straton, *Electromagnetic Theory* (McGraw-Hill, New York, 1941), p. 392.
[34] J. O. Vasseur, B. Djafari-Rohani, L. Xobrzynski, M. S. Kushwaha, and P. Halevi, J. Phys. Condens. Mater. **6**, 8759 (1994).
[35] L. D. Landau and E. M. Lifshitz, *Theory of Elasticity*, 3rd ed. (Pergamon, Oxford, 1986).
[36] M. Kafesaki, M. M. Sigalas, and E. N. Economou, Solid State Commun. **96**, 285 (1995).